



Synthesis and electrochemical characterization of $\text{Sr}_2\text{Fe}_{1.5}\text{Mo}_{0.5}\text{O}_6-\text{Sm}_{0.2}\text{Ce}_{0.8}\text{O}_{1.9}$ composite cathode for intermediate-temperature solid oxide fuel cells



Ningning Dai, Zhongliang Lou, Zhenhua Wang, Xiaoxi Liu, Yiming Yan, Jinshuo Qiao*,
Taizhi Jiang, Kening Sun*

School of Chemical Engineering and Environment, Beijing Institute of Technology, Beijing 100081, China

HIGHLIGHTS

- Investigation on nanostructure and performance of materials SFM–SDC as IT-SOFC cathodes.
- SFM–SDC40 exhibits the lowest R_p in these cathodes.
- Decreased R_p of the SDC/SFM–SDC bi-layer cathodes observed.
- Significantly improved cell power performance demonstrated with SDC/SFM–SDC cathodes.

ARTICLE INFO

Article history:

Received 10 April 2013

Received in revised form

28 May 2013

Accepted 28 May 2013

Available online 8 June 2013

Keywords:

Solid oxide fuel cell

Composite cathode

Interlayer

Polarization resistance

ABSTRACT

Nanoporous composite oxides $\text{Sr}_2\text{Fe}_{1.5}\text{Mo}_{0.5}\text{O}_6-\text{Sm}_{0.2}\text{Ce}_{0.8}\text{O}_{1.9}$ (SFM–SDC) have been prepared by a facile one-step method as cathode for intermediate-temperature solid oxide fuel cells (IT-SOFCs). The SFM–SDC composite materials have been characterized by X-ray diffraction (XRD), scanning electron microscopy (SEM), scanning transmission electron microscopy (STEM) and electrochemical impedance spectroscopy (EIS). The EIS results exhibit that SFM–SDC40 (wt% 60:40) cathode has encouraging electrochemical performance with low polarization resistance (R_p) on YSZ (Y_2O_3 -stabilized ZrO_2) electrolyte. Subsequently, bi-layer cathodes SDC/SFM–SDC are fabricated, and excellent electrochemical performance of such composite cathodes are observed. We demonstrate that the SDC interlayer significantly decreases the R_p of cathode and accelerates the charge transfer process. As a result, the R_p of the SDC/SFM–SDC40 bi-layer cathodes is almost 50% less than that of SFM–SDC40 cathode on YSZ electrolyte at 800 °C, and R_p is only 0.11 Ω cm². Compared with single cells without an interlayer, the anode-supported single cells with SDC interlayer exhibit enhancement in overall power performance.

© 2013 Elsevier B.V. All rights reserved.

1. Introduction

Solid oxide fuel cells (SOFCs) are considered to be ecocentric devices that generate electricity by electrochemical reaction with higher efficiency than conventional methods for producing electricity. Current researches have primarily focused on the development of intermediate-temperature SOFCs (IT-SOFCs), which are operated within a temperature range of 600–800 °C to thereby diminish the premature aging of electrode materials, thus improving the durability, stability, and reliability of the SOFCs [1–5].

However, with the decrease of operating temperature, the performance of cathodes is becoming a limiting factor in determining the overall cells performance, particularly for anode-supported IT-SOFCs, because the electrochemical activity of the cathode may dramatically decline at lower operating temperature. Two approaches have been proposed to address this concern. One is to develop new cathode materials with higher performance such as $\text{Ba}_2\text{Bi}_{0.1}\text{Sc}_{0.2}\text{Co}_{1.7}\text{O}_{6-x}$ [6,7] and the other method is to optimize the microstructure by using novel strategies [8,9].

In addition, developing composite cathodes has also recently proved to be an effective strategy to improve the electrochemical performance for IT-SOFCs. The composite cathode can achieve higher oxygen reduction reaction (ORR) activity compared with single-phase cathode, because the extra phase provides additional electronic or ionic conductivity [10–12]. For example, we

* Corresponding authors. Tel./fax: +86 010 6891 8696.

E-mail addresses: qjinshuo@bit.edu.cn (J. Qiao), [\(K. Sun\).](mailto:bitkeningsun@yahoo.com.cn)

investigated the performance of $\text{La}_{0.8}\text{Sr}_{0.2}\text{MnO}_3$ –YSZ (LSM–YSZ) composite cathode on YSZ electrolyte. The LSM–YSZ cathode displayed polarization resistance (R_p) that decreased from $0.396 \Omega \text{ cm}^2$ (LSM cathode) to $0.246 \Omega \text{ cm}^2$ at 800°C [13]. Furthermore, the composite cathodes of $\text{La}_{0.6}\text{Sr}_{0.4}\text{Co}_{0.2}\text{Fe}_{0.8}\text{O}_3$ – $\text{Ce}_{0.8}\text{Gd}_{0.2}\text{O}_3$ (LSCF–GDC) were also studied by Barnett et al. [14] and the value of R_p was as low as $0.33 \Omega \text{ cm}^2$ at 600°C . All these composite materials show a significant enhancement of the electrochemical performance of single-phase cathode. Moreover, since the ORR occurs at the triple-phase boundary (TPB) [15], high specific surface area and adequate porosity of cathode are desired to obtain large TPBs [16–18]. Therefore, porous nanocomposite cathode materials are primarily required to improve the electrochemical performance. Herein we describe the preparation of nanoporous composite material for IT-SOFC cathode by facile strategy.

Recently, electrodes based on $\text{Sr}_2\text{Fe}_{1.5}\text{Mo}_{0.5}\text{O}_6$ (SFM) were proven to be extremely efficient for IT-SOFCs [19,20]. SFM has been used as cathode and anode material in a symmetrical configuration, exhibiting remarkable electrocatalytic activity for oxygen reduction or fuels oxidation while demonstrating high ionic and electronic conductivity [21]. It is known that $\text{Sm}_{0.2}\text{Ce}_{0.8}\text{O}_{1.9}$ (SDC) has not only ideal for catalytic activity for electrochemical reaction but also excellent oxygen ion-conducting capacity. The oxygen ion conductivity of SDC is 0.041 S cm^{-1} at 700°C [22]. The introduction of oxygen ion-conducting materials into electrodes can promote the ionic exchange processes and expand the electrochemical reaction length along the electrode/electrolyte and electrode/gas interfaces, thus reducing the polarization losses [23].

In this work, $\text{Sr}_2\text{Fe}_{1.5}\text{Mo}_{0.5}\text{O}_6$ – $\text{Sm}_{0.2}\text{Ce}_{0.8}\text{O}_{1.9}$ (SFM–SDC) composite materials with different ratio of SFM to SDC were prepared by a one-step combustion technology which was facile and timesaving. Phase structure and microstructure of the materials were characterized with X-ray diffraction (XRD) and scanning electron microscopy (SEM). Electrochemical impedance spectroscopy (EIS) was measured to obtain systematic electrochemical information about the composite materials on YSZ electrolyte. Single cells were also fabricated and tested to evaluate the performance of the single SFM–SDC layer cathode and SDC/SFM–SDC bi-layer cathodes.

2. Experimental

2.1. Materials preparation

The materials used in this work include SFM–SDC, SDC, 8% Y_2O_3 -stabilized ZrO_2 (8YSZ, Tosoh Co., Japan) and NiO (High Purity Chemicals, Japan). SFM–SDC composite powders were synthesized using a one-step combustion method. Stoichiometric amounts of $\text{Sr}(\text{NO}_3)_2$, $\text{Fe}(\text{NO}_3)_3 \cdot 9\text{H}_2\text{O}$, $(\text{NH}_4)_6\text{Mo}_7\text{O}_{24} \cdot 4\text{H}_2\text{O}$, $\text{Sm}(\text{NO}_3)_3 \cdot 6\text{H}_2\text{O}$ and $\text{Ce}(\text{NO}_3)_3 \cdot 6\text{H}_2\text{O}$ were used as the metal precursors. Glycine and citric acid were used to assist combustion. The mole ratio of glycine and citric acid to the total metal cations was 2:1.5:1. The synthesis process is illustrated in Fig. 1. Glycine and the metal precursors were dissolved in deionized water under stirring at 80°C . Citric acid was added gradually to the above suspension, which was subsequently dried at 80°C to form a transparent gel. The resultant gel was heated to 250°C until the composite gel combusted. The as-prepared ash was calcined at 800°C for 2 h and 1000°C for 5 h in air to obtain pure SFM–SDC composite powders. The composite materials SFM–SDC (wt% SFM:SDC = 70:30, 60:40, 50:50, 40:60, and hereafter are identified as SFM–SDC30, SFM–SDC40, SFM–SDC50, SFM–SDC60, respectively) were investigated. SDC powders for this work were prepared by sol-gel technology. In order to measure the thermal expansion coefficient (TEC) of the SFM–SDC



Fig. 1. Schematic representation for preparation of porous SFM–SDC composite materials by one-step combustion method.

materials, the composite powders were uniaxially pressed into stick form and then fired 1200°C for 5 h to obtain dense bar pellets.

2.2. Fabrication of SOFCs with SFM–SDC cathodes

The SFM–SDC composite cathode performance was studied by assembling cells. NiO–YSZ anode-supported cell with YSZ electrolyte film was prepared by co-tape casting technology [30]. Generally, the thickness of the anode and the electrolyte film produced by this method is approximately $700 \mu\text{m}$ and $10 \mu\text{m}$, respectively. SDC interlayer was screen-printed onto YSZ electrolyte and then sintered at 1400°C for 8 h. The obtained SDC interlayer was approximately $4 \mu\text{m}$ thick. The SFM–SDC composite powders were then screen-printed directly onto the YSZ electrolyte or onto the SDC interlayer, and calcinated at 1000°C for 2 h to obtain the NiO–YSZ/YSZ/SFM–SDC and NiO–YSZ/YSZ/SDC/SFM–SDC single cells. The cathode area was approximately 0.2 cm^2 and the thickness was approximately $10 \mu\text{m}$. The dense YSZ electrolyte substrates were prepared by uniaxially pressing at 300 MPa and sintering at 1400°C for 6 h. The three-electrode cells were assembled in order to measure the EIS for the composite cathodes, which has been described elsewhere [24].

2.3. Characterization of SFM–SDC cathode

The phase structure of the SFM–SDC materials was determined by XRD (X'Pert PRO MPD). The microstructure of the composite powder and the prepared electrode was observed using a scanning electron microscope (SEM, FEI QUANTA-250) and scanning transmission electron microscopy (STEM, FEI TECNAI F30). The TEC was measured using a dilatometer (Netsch DIL 402C) from 40°C to 1000°C . PARSTAT 2273 have been used to measure the EIS for SFM–SDC cathodes. The single cells were tested with humidified hydrogen (3 vol% H_2O) as the fuel at a flow rate of 50 mL min^{-1} and with ambient air as the oxidant. The current–voltage curves of the cells were recorded using an Arbin Instruments tester (Fuel Cell Test System, FCTS).

3. Results and discussion

3.1. SFM–SDC composite cathode with different ratio of SFM to SDC

3.1.1. Structural stability of SFM–SDC powders

The XRD patterns of the as-synthesized SFM–SDC powders by one-step method with different ratio of SFM to SDC are shown in Fig. 2. XRD analysis displayed that cubic perovskite SFM and fluorite SDC phase structures were obtained in the SFM–SDC composite materials, in which the diffraction of impurity was not observed. This indicates that the SFM–SDC composite at different mass ratios are fully consist of pure SFM and SDC phase. The XRD results strongly indicate that one-step combustion is a feasible method to synthesize SFM–SDC composite materials.

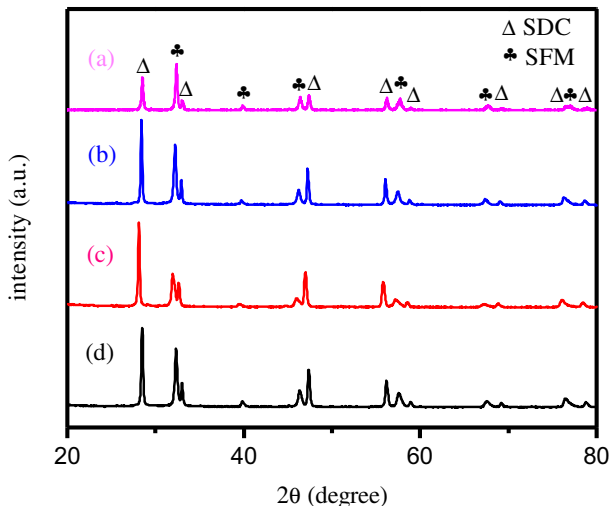


Fig. 2. XRD of SFM–SDC samples at various component of (a) SFM–SDC30, (b) SFM–SDC40, (c) SFM–SDC50, (d) SFM–SDC60.

3.1.2. Microstructure of SFM–SDC composite powders

Fig. 3 presents the SEM micrographs of the SFM–SDC composite powders with different SDC content. These composite materials displayed porous microstructure and all the samples showed uniform morphology. A large number of layered interconnecting pores generated by pyrolysis of glycine and citric acid were found to be distributed homogeneously across the SFM–SDC composite materials. The average size of the pores is estimated to be approximately 1 μm. From inset of Fig. 3b, it can be observed that the SFM and SDC grains were nano-sized. However, it was difficult to recognize SDC amongst the SFM particles, which may because both SDC and SFM grains are nanoscale and distributed homogeneously. In order to

obtain more information of the particles sizes and the distribution in two phases, the morphology of SFM–SDC40 material was further investigated by using STEM. As shown in Fig. 4, SFM and SDC particles were clearly distinguished. It was observed that the SDC particles were finer and smaller, about 10–100 nm in diameter, than the SFM particles (100–200 nm). As a consequence, it is believed that such microstructure of SFM–SDC40, which combines both a high-porosity scaffold and nanoparticles, could facilitate gas diffusion, electrochemical reaction, electron and oxygen ion transport in the cathode [25,26].

3.1.3. Microstructure of SFM–SDC composite cathode

All the prepared SFM–SDC composite cathodes have similar microstructure on YSZ electrolyte. For example, the SEM micrographs of surface and cross-section for SFM–SDC40 composite cathode and elemental line profiles have been presented in Fig. 5. As shown, SFM–SDC40 cathode maintained the porous network nanostructure after sintered at 1000 °C for 2 h (Fig. 5a). Such a cathode microstructure with adequate porosity is favorable for oxygen transportation, as it provides rich reaction sites for electrochemical oxygen reduction and multiple paths for electrons transport in the electrode. Therefore, the composite cathode consisted of nano-sized SFM and SDC particles may contribute to better overall electrochemical performance.

Fig. 5b shows the cross-section micrograph of an interface of the tri-layer cell (NiO–YSZ/YSZ/SFM–SDC40). It appeared that the SFM–SDC40 cathode and the YSZ electrolyte were adhered to each other without any sign of cracks and delamination. The TEC of SFM–SDC40 was further measured as $13.58 \times 10^{-6} \text{ K}^{-1}$, which is quite approach to that of YSZ ($10.8 \times 10^{-6} \text{ K}^{-1}$) [27] over the temperature range of 40–800 °C, indicating that the SFM–SDC composite cathode and the conventional electrolyte YSZ have good thermal compatibility. Fig. 5c displays the elemental line profiles of the element distribution of Ce, Sm, Sr, Fe, Mo, Zr and Y in the

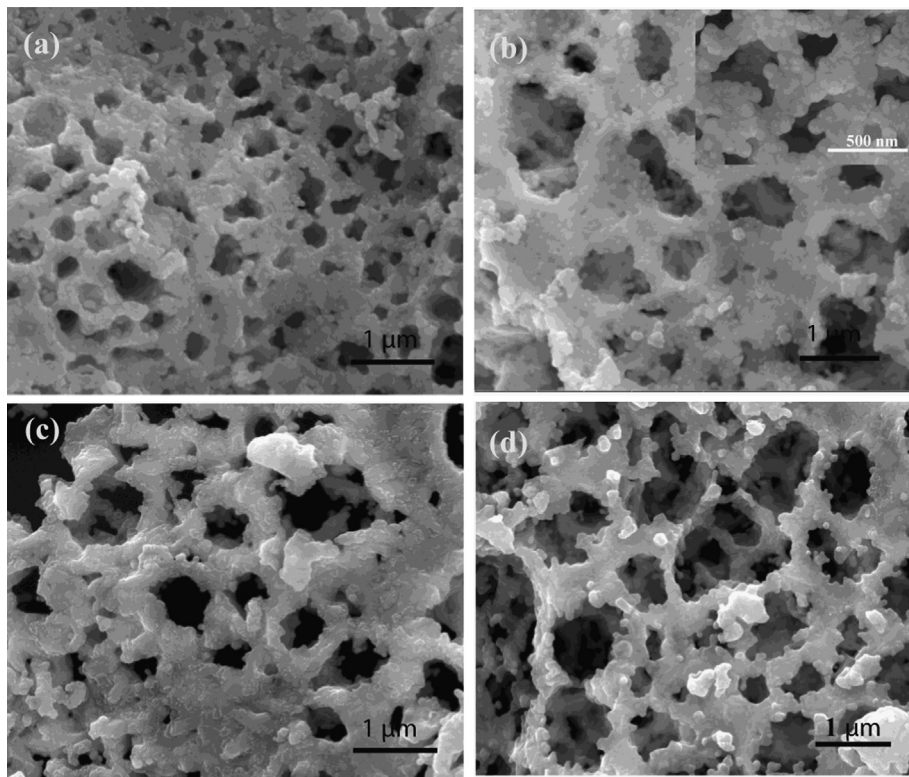


Fig. 3. SEM micrographs of SFM–SDC powders of (a) SFM–SDC30, (b) SFM–SDC40, (c) SFM–SDC50, (d) SFM–SDC60.

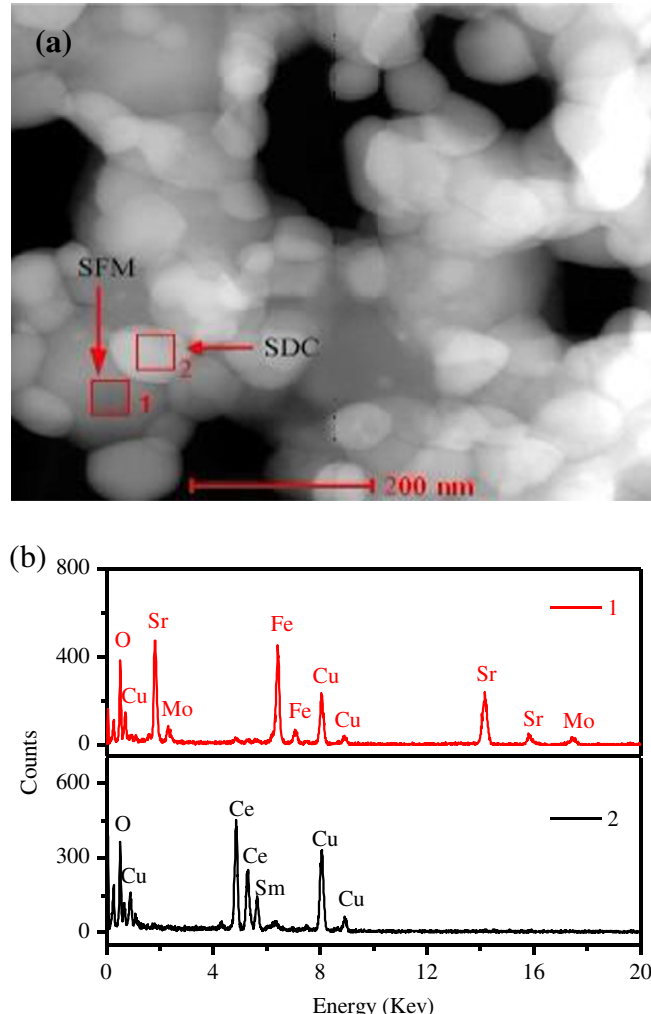


Fig. 4. STEM (a) patterns of SFM–SDC40 powders and related EDX curves (b) scanning the area of box in (a).

cathode and electrolyte regions. No elemental interpenetration between the layers was observed, indicating that no solid-state reaction occurred at the interface between SFM–SDC and YSZ after firing at 1000 °C for 2 h in air.

3.1.4. EIS of SFM–SDC composite cathodes with different ratio of SFM to SDC

In order to investigate effect of SDC content on the performance of SFM–SDC composite cathodes, EIS for SFM–SDC cathodes with different ratio of SFM to SDC on YSZ electrolyte were measured with three-electrode system in atmospheric air. The typical impedance spectra for SFM–SDC composite cathodes can be fitted with the equivalent circuit $L R_{\Omega} (Q_H R_H) (Q_L R_L)$. For comparison, the R_{Ω} was omitted in the Nyquist plots and the fitting results of SFM–SDC cathodes, shown in Fig. 6. The impedance spectra consist of two arcs. The high-frequency resistance (R_H) represented the charge transfer at the electrode/electrolyte interface from the movement of oxygen anions [28], and the low-frequency resistance (R_L) was related to oxygen surface adsorption and diffusion in the cathode [29,30]. The total polarization resistance of cathode, R_p , is the sum of R_H and R_L . Fig. 6a shows the content of SDC in SFM–SDC cathodes has a significant effect on R_p of these composite cathodes at operating temperature range from 650 °C to 800 °C. When the SDC content increased from 30 wt% to 40 wt% in SFM–SDC cathode, the

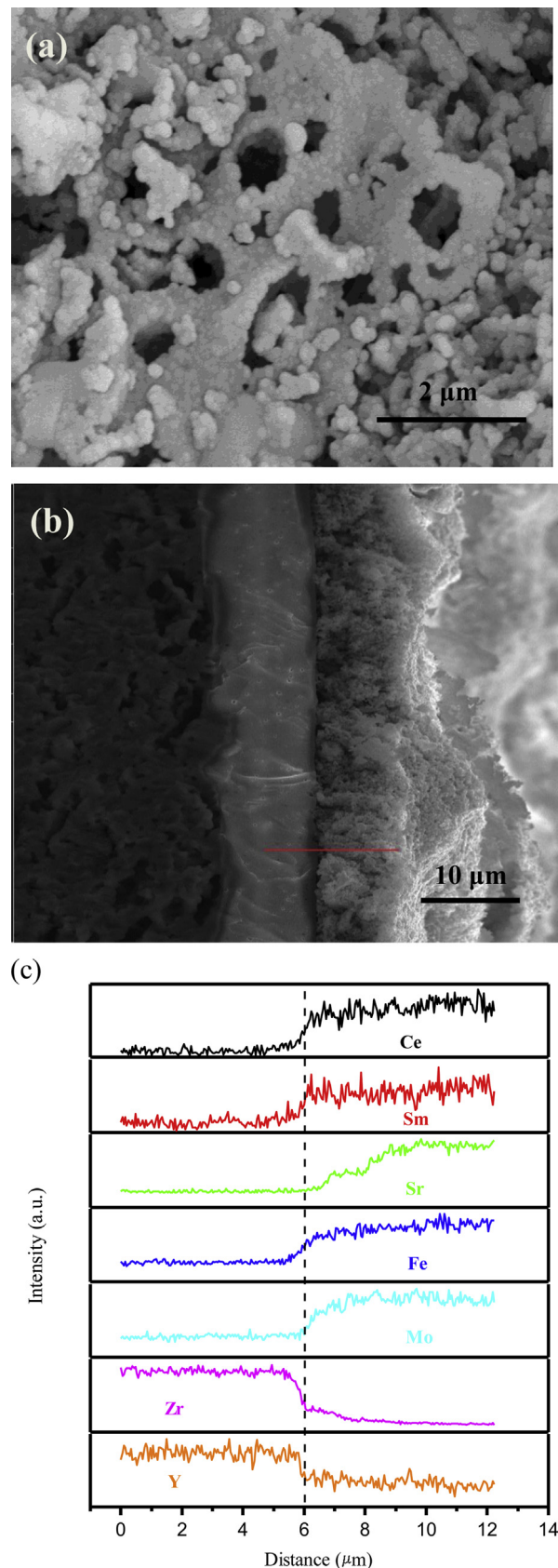


Fig. 5. (a) Surface and (b) cross-section SEM micrograph and (c) EDX linear scan analysis of the relative elemental distribution of the fuel cell with SFM–SDC40 composite cathode on YSZ electrolyte.

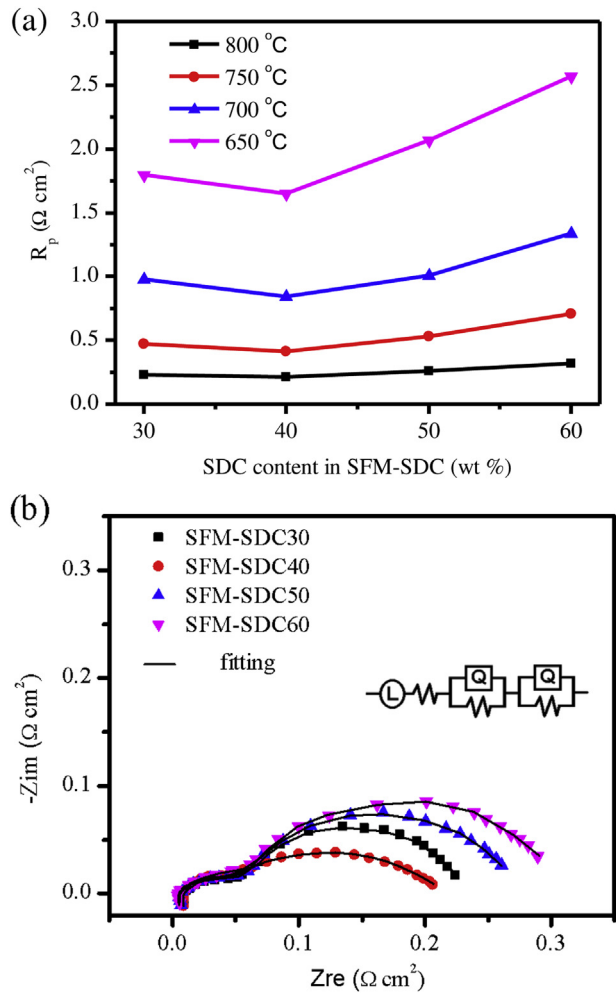


Fig. 6. (a) Dependence of R_p for SFM–SDC composite cathodes with different SDC content at 650–800 °C in air. (b) Impedance spectra of the SFM–SDC cathodes with different ratio of SFM to SDC measured on YSZ electrolyte at 800 °C in air.

Table 1
EIS fitting results of SFM–SDC composite cathodes on YSZ electrolyte at 800 °C.

Cathodes	R_H ($\Omega \text{ cm}^2$)	R_L ($\Omega \text{ cm}^2$)	R_p ($\Omega \text{ cm}^2$) ($R_p = R_H + R_L$)
SDC/SFM–SDC30	0.0474	0.192	0.239
SDC/SFM–SDC40	0.0213	0.181	0.202
SDC/SFM–SDC50	0.0589	0.203	0.262
SDC/SFM–SDC60	0.0814	0.228	0.309

R_p value of the cathode decreased. This indicates that higher SDC content resulted in better performance for the composite cathode, which can be explained by the fact that SDC nanoparticles which could accelerate the transport of oxygen ions through the electrode. Concurrently, the well-distributed SFM and SDC particles in

cathode can significantly extend the TPBs for the electrochemical reaction of oxygen, and consequently reduce the electrode polarization resistance. When the content of SDC in SFM–SDC cathode was 40 wt%, the R_p of SFM–SDC cathode were 0.83, 0.41, 0.20 $\Omega \text{ cm}^2$ at 700, 750, 800 °C. However, when the SDC content in SFM–SDC cathodes increased to 50 wt% and 60 wt%, the R_p apparently increased, which presumably is caused by the decrease of electrochemical reaction sites with the decrease of SFM. On the other hand, the electrons transport channels of SFM were blocked because of the reduced connectivity of SFM with the increase of SDC content. EIS measurement results exhibited that SFM–SDC40 cathode presented the lowest R_p in these composite cathodes at 650–800 °C.

The EIS for SFM–SDC composite cathodes with different ratio of SFM to SDC studied at 800 °C on YSZ electrolyte are shown in Fig. 6b. The primary fitting results of these cathodes were achieved with the equivalent circuit $L R_Q (Q_H R_H) (Q_L R_L)$ as shown in Table 1. It can be seen that the R_L value of 0.181 $\Omega \text{ cm}^2$ for SFM–SDC40 was lower than that of SFM–SDC60 ($R_L = 0.228 \Omega \text{ cm}^2$). The lower R_L value could be attributed to the SFM–SDC40 cathode providing proper gas diffusion channels and reducing the resistance of oxygen surface adsorption and diffusion. When SDC content is 40 wt%, the $R_H = 0.0213 \Omega \text{ cm}^2$, which is lower than other composite cathodes demonstrating that adding 40 wt% SDC can significantly improve the charge exchange kinetics of the cathode. The high-frequency process is directly linked with the TPB. It was assumed that the composite cathode with 40 wt% SDC has a larger TPB length which indicates more catalytic reaction sites and more parallel oxygen ion incorporation paths in the cathode. This result can be further explained by the binary-random-sphere packing model and percolation theory, which the maximum TPB length is a function of the two-phase composition and particles size ratio of electronic to oxygen ionic conductor [31]. When the particle size of the ionic phase is smaller than the electronic phase, the maximum TPB length can be obtained at a content of a volume fraction of the ionic conductor being less than 50%. As shown in the STEM image (Fig. 4), the particle size of the ionic phase SDC is apparently smaller than the electronic phase SFM. For the optimized composition SFM–SDC40 with 40 wt% SDC, it is readily apparent that the volume of ionic phase SDC was less than 50%, although it is not possible to measure the accurate volume of SFM and SDC because of the one-step *in-situ* synthesis strategy. The volume ratio of SFM and SDC particles in SFM–SDC40 is consistent with theoretical predictions.

3.2. Effect of SDC interlayer on SFM–SDC cathodes

3.2.1. Effect of SDC interlayer on the impedance of SFM–SDC cathodes

EIS of SFM–SDC cathodes on YSZ electrolyte with SDC interlayer at 650–800 °C were previously studied. The polarization resistances of these SDC/SFM–SDC cathodes with SDC interlayer on YSZ electrolyte were further investigated as shown in Table 2. The electrochemical performance of SDC/SFM–SDC40 were better than other ratio of bi-layer cathodes under same test condition, and the values of R_p were 0.52, 0.27, 0.11 $\Omega \text{ cm}^2$ at 700, 750, 800 °C,

Table 2

Results of fitted polarization resistance (R_p) of SFM–SDC cathodes on YSZ electrolyte with SDC interlayer at 650–800 °C.

Temperature (°C)	SDC/SFM–SDC30 ($\Omega \text{ cm}^2$)	SDC/SFM–SDC40 ($\Omega \text{ cm}^2$)	SDC/SFM–SDC50 ($\Omega \text{ cm}^2$)	SDC/SFM–SDC60 ($\Omega \text{ cm}^2$)
800	0.16	0.11	0.21	0.30
750	0.34	0.27	0.44	0.58
700	0.61	0.52	0.82	1.03
650	1.32	1.21	1.58	1.84

respectively. In addition, the R_p of the SDC/SFM–SDC bi-layer cathodes were lower than SFM–SDC single layer cathodes on YSZ electrolyte. Compared with SFM–SDC40 single layer cathode, the R_p of SDC/SFM–SDC40 bi-layer cathodes decreased more than 35% at both 700 and 750 °C, and decrease ~50% at 800 °C.

The EIS of SFM–SDC40 composite cathode without and with SDC interlayer on YSZ electrolyte at 800 °C are given in Fig. 7 and Table 3. From Fig. 7, it can be seen that the EIS for the SFM–SDC40 cathode on YSZ electrolyte consisted of two arcs, but that of the SDC/SFM–SDC40 bi-layer cathodes seemed to exhibit only a single arc. In Fig. 7a, the low-frequency arc was larger than the high-frequency arc, and the peak frequency was 1.5 Hz, which indicates that gas adsorption, diffusion processes were limiting factors in the reactions at the SFM–SDC40 single layer cathode. The EIS for the SDC/SFM–SDC40 bi-layer cathodes consisted of a single arc as shown in Fig. 7b, and the peak frequency was also 1.5 Hz. The single arc corresponded to gas adsorption and diffusion processes, and the disappearances of a high-frequency arc were ascribed to the introduction of the SDC interlayer. It is evident that the relatively thin SDC interlayer provides the desired catalytic activity and excellent ion transport capability. Moreover, the R_Ω of the SDC/SFM–SDC40 bi-layer cathodes ($0.236 \Omega \text{ cm}^2$) was significantly lower than that of the SFM–SDC40 cathode ($0.359 \Omega \text{ cm}^2$) as shown in Table 3. This was probably because the SDC interlayer improved adhesion between the electrolyte/interlayer and the cathode.

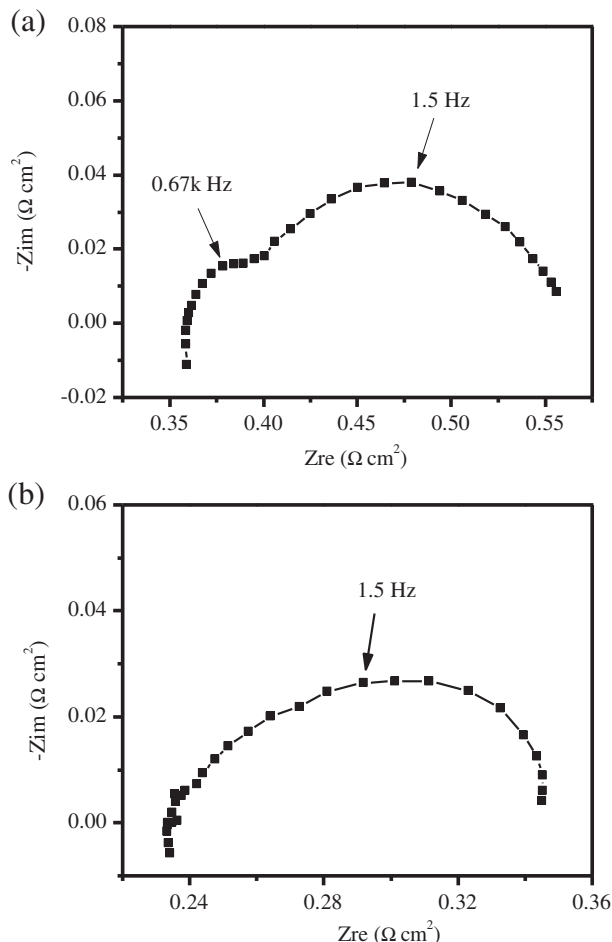


Fig. 7. EIS of SFM–SDC40 composite cathodes on YSZ electrolyte at 800 °C: (a) SFM–SDC40 single layer cathode and, (b) SDC/SFM–SDC40 bi-layer cathodes.

Table 3

EIS fitting results of SFM–SDC40 and SDC/SFM–SDC40 cathodes on YSZ electrolyte at 800 °C.

Cathodes	$R_\Omega (\Omega \text{ cm}^2)$	$R_H (\Omega \text{ cm}^2)$	$R_L (\Omega \text{ cm}^2)$	$R_p (\Omega \text{ cm}^2)$ ($R_p = R_H + R_L$)
SFM–SDC40	0.359	0.0213	0.181	0.202
SDC/SFM–SDC40	0.236	—	0.113	0.113

3.2.2. Effect of SDC interlayer on the discharge performance of the cells

Fig. 8a and b displays the I – V and I – P curves of NiO–YSZ/YSZ anode-supported cells with SFM–SDC40 single layer cathode and

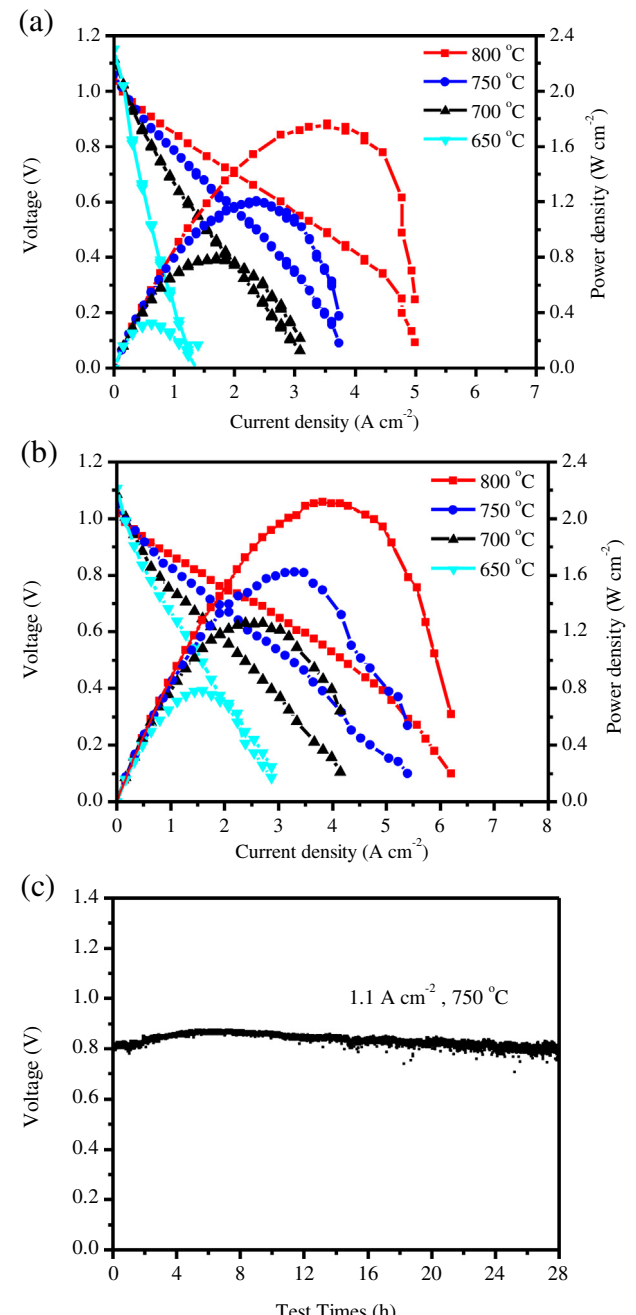


Fig. 8. (a) I – V and I – P plots of the cell NiO–YSZ/YSZ/SFM–SDC40 at 650–800 °C, (b) I – V and I – P plots of the cell NiO–YSZ/YSZ/SDC/SFM–SDC40 at 650–800 °C, (c) the stability test for NiO–YSZ/YSZ/SDC/SFM–SDC40 single cell at 750 °C.

SDC/SFM–SDC40 bi-layer cathodes, operating at 650–800 °C. Both cells possessed an open circuit voltage (OCV) close to the theoretical value, which demonstrated that the YSZ electrolyte was sufficiently dense. However, the maximum power densities of the two cells differ clearly. As shown in Fig. 8a, the cells with single SFM–SDC40 layer cathode demonstrated maximum power densities of 0.33, 0.79, 1.21, 1.77 W cm⁻² at 650, 700, 750, 800 °C, respectively. By comparison, the peak power densities of the cells with the SDC/SFM–SDC40 bi-layer cathodes were 0.78, 1.26, 1.62, 2.11 W cm⁻² at 650, 700, 750, 800 °C (Fig. 8b). These results suggest that the addition of SDC interlayer can successfully improve the electrochemical performance of cells.

The NiO–YSZ/YSZ/SFM–SDC40 single cell showed stable performance with no obvious degradation in 28 h under a constant current density of 1.1 A cm⁻² at 750 °C, as shown in Fig. 8c. These results indicate that SFM–SDC prepared by one-step method is an attractive cathode material for IT-SOFCs. Concurrently, it was verified that SDC interlayer applied in NiO–YSZ/YSZ/SFM–SDC40 cells can effectively enhance the performance and stability.

4. Conclusions

SFM–SDC composite materials were prepared through one-step combustion method. The SFM and SDC particles were homogeneously dispersed, and nanoporous network structure in these samples was formed. The EIS of SFM–SDC composite cathodes with different ratio of SFM to SDC were investigated. The R_p values of SFM–SDC40 composite cathode were lower than that of composite cathodes of other ratio. The introduction of SDC interlayer can apparently reduce the R_p of the SFM–SDC cathode, and enhance electrochemical performance and improve the stability of the cells. Compared with SFM–SDC40 cathode, the R_p values of SDC/SFM–SDC40 bi-layer cathodes reduced approximately 35–50%. The anode-supported single cells with SDC interlayer also demonstrate significantly enhanced power performance in a temperature range of 650–800 °C compared with the cells without SDC interlayer. The maximum power densities of NiO–YSZ/YSZ/SFM–SDC and NiO–YSZ/YSZ/SDC/SFM–SDC were 0.33 and 0.78 W cm⁻² at 650 °C, 1.77 and 2.11 W cm⁻² at 800 °C, respectively. In conclusion, we have demonstrated that SFM–SDC composite is a potential cathode for intermediate-temperature SOFCs and that the SDC interlayer between YSZ electrolyte and SFM–SDC cathode can effectively improve cell performance.

Acknowledgments

This work is financial supported by National Natural Science Foundation of China (Grant Nos. 21006015 and 21070623) and also supported by the Foundation of Beijing Key Laboratory for Chemical Power Source and Green Catalysis, contract No. 2013CX02031.

References

- [1] B.C.H. Steele, A. Heinzel, *Nature* 414 (2001) 345–352.
- [2] J.C. Ruiz-Morales, D. Marrero, C. Savaniud, S.N. Savvin, *Energy Environ. Sci.* 3 (2010) 1670–1681.
- [3] L. Yang, S. Wang, K. Blinn, M.F. Liu, Z. Liu, Z. Cheng, M.L. Liu, *Science* 326 (2009) 126–129.
- [4] A. Orera, P.R. Slater, *Chem. Mater.* 22 (2010) 675–690.
- [5] A.J. Jacobson, *Chem. Mater.* 22 (2010) 660–674.
- [6] W. Zhou, J. Sunarso, Z.G. Chen, L. Ge, J. Motuzas, J. Zou, G.X. Wang, A. Julbe, Z.H. Zhu, *Energy Environ. Sci.* 4 (2011) 872–875.
- [7] W. Zhou, J. Sunarso, J. Motuzas, F.L. Liang, Z.G. Chen, L. Ge, S.M. Liu, A. Julbe, Z.H. Zhu, *Chem. Mater.* 23 (2011) 1618–1624.
- [8] J.H. Choi, J.H. Jang, J.H. Ryu, S.M. Oh, *J. Power Sources* 87 (2000) 92–100.
- [9] J.H. Choi, J.H. Jang, S.M. Oh, *Electrochim. Acta* 46 (2001) 867–874.
- [10] F.L. Liang, W. Zhou, B. Chi, J. Pu, S.P. Jiang, L. Jian, *Int. J. Hydrogen Energy* 36 (2011) 7670–7676.
- [11] B.M. An, W. Zhou, Y.M. Guo, R. Ran, Z.P. Shao, *Int. J. Hydrogen Energy* 35 (2010) 5601–5610.
- [12] E. Perry Murray, S.A. Barnett, *Solid State Ionics* 143 (2001) 265–273.
- [13] J.H. Piao, K.N. Sun, N.Q. Zhang, S. Xu, *J. Power Sources* 175 (2008) 288–295.
- [14] E.P. Murray, M.J. Sever, S.A. Barnett, *Solid State Ionics* 148 (2002) 27–34.
- [15] R.R. Peng, T.Z. Wu, W. Liu, X.Q. Liu, G.Y. Meng, *J. Mater. Chem.* 20 (2010) 6218–6225.
- [16] D.H. Dong, D. Li, X.Y. Zhang, Z.L. Chai, K. Wang, C.Z. Li, D.Y. Zhao, H.T. Wang, *J. Mater. Chem.* 20 (2010) 1122–1126.
- [17] E.C. Brown, S.K. Wilke, D.A. Boyd, D.G. Goodwin, S.M. Haile, *J. Mater. Chem.* 20 (2010) 2190–2196.
- [18] M.J. Zhi, N. Mariani, R. Gemmen, K. Gerdes, N.Q. Wu, *Energy Environ. Sci.* 4 (2011) 417–420.
- [19] G.L. Xiao, Q. Liu, F. Zhao, L. Zhang, C.R. Xia, F.L. Chen, *J. Electrochem. Soc.* 158 (2011) B455–B460.
- [20] Q. Liu, D.E. Bugaris, G.L. Xiao, M. Chmara, S.G. Ma, H.-C.Z. Loyer, M.D. Amirdis, F.L. Chen, *J. Power Sources* 196 (2011) 9148–9153.
- [21] Q. Liu, X.H. Dong, G.L. Xiao, F. Zhao, F.L. Chen, *Adv. Mater.* 22 (2010) 5478–5482.
- [22] H. Yahiro, K. Eguchi, H. Arai, *Solid State Ionics* 36 (1989) 71–75.
- [23] S.B. Alder, *Solid State Ionics* 111 (1998) 125–134.
- [24] Q. Fu, K.N. Sun, N.Q. Zhang, S.R. Le, X.D. Zhu, J.H. Piao, *J. Solid State Electrochem.* 13 (2009) 455–467.
- [25] Y. Liu, S.W. Zha, M.L. Liu, *Adv. Mater.* 16 (2004) 256–260.
- [26] T.Z. Sholkapper, H. Kurokawa, C.P. Jacobson, S.J. ViSco, L.C. De Jonghe, *Nano Lett.* 7 (2007) 2136–2141.
- [27] H. Liu, X. Zhu, M. Cheng, Y. Cong, W. Yang, *Chem. Commun.* 47 (2011) 2378–2380.
- [28] S.P. Jiang, S.P.S. Badwal, *Solid State Ionics* 123 (1999) 209–224.
- [29] S.B. Adler, J.A. Lane, B.C.H. Steele, *J. Electrochem. Soc.* 143 (1996) 3554–3564.
- [30] S.B. Adler, *Solid State Ionics* 135 (2000) 603–612.
- [31] X.J. Chen, S.H. Chan, K.A. Khor, *Electrochim. Acta* 49 (2004) 1851–1861.